Pre-Emission Study of Photoelectron Dynamics in a GaAs/AlGaAs Photocathode

Hemang Jani, *Student Member, IEEE*, Liang Chen, and Lingze Duan, *Senior Member, IEEE*

***Abstract*— Understanding the carrier dynamics in III-V semiconductor photocathodes is of great importance to the development of many novel optoelectronic systems such as low-light imagers and coherent x-ray sources. Past experimental effort to study ultrafast response of GaAs photocathodes has relied exclusively on post-photoemission measurement, i.e. via characterization of the temporal properties of emitted electron bunches. Such an indirect approach is not only difficult to achieve experimentally but also liable to sample surface conditions when assessing key carrier dynamics such as photoelectron diffusion and decay. In this report, we present a pre-photoemission investigation of photoelectron transport and population decay in a GaAs/AlGaAs photocathode based on pump-probe transient reflectometry. By measuring the ultrafast behaviors of reflectivity after the excitation of a femtosecond optical pulse, we are able to evaluate the transient evolution of photoelectron population near the device surface, which provides a direct picture of electron diffusion and decay. A carrier diffusion model shows excellent agreement with experiment. Experiment-theory comparisons also suggests a diffusion coefficient much greater than some of the post-photoemission predictions. In addition, the free-electron population decay near the surface is found to be of bi-exponential nature. Possible physical mechanisms underlying these decay lifetimes are discussed.**

***Index Terms*— Carrier dynamics, GaAs, negative electron affinity photocathode, pump-probe method, transient reflection, ultrafast optics, ultrafast spectroscopy.**

I. Introduction

III-V SEMICONDUCTOR photocathodes with negative electron affinity (NEA) have attracted a lot of research interest over the last two decades owing to their high quantum efficiency and low dark emission, which are crucial parameters for low-light applications such as photomultipliers, low-energy electron microscopes, and night-vision image intensifiers [1]–[6]. The development of the next-generation free-electron lasers and coherent X-ray sources also puts such photocathodes in high demand as the ideal electron-beam injector with low thermal emittance, high average current, and good polarization purity [7]–[12]. More recently, the emerging concept of space X-ray communication (XCOM) prompts new interest in transmission-mode semiconductor photocathodes [13] and similar structures are also gaining interests as efficient solar energy converters [14], [15]. Furthermore, key research areas in photocathodes, e.g., quantum efficiency enhancement, carrier escape time, etc., also draw interest from related fields such as silicon photonics [16], [17] and wide-bandgap light emitting diode [18].

There has been a lot of work dedicated to the improvement of the design and the performance of III-V photocathodes [19]–[22]. The majority of these prior efforts have focused on the steady-state parameters such as spectral response and quantum efficiency of GaAs-based photocathodes [23]–[27]. The dynamic properties of these photocathodes have received relatively less attention [9], [28], [29]. However, growing demand for time-resolved electron beams in recent years has prompted a surge of interest in carrier dynamics inside GaAs photocathodes [8], [9], [28], [30]–[34]. Understanding the transient behaviors of photoelectrons, such as their transport and population decay upon the excitation of ultrafast laser pulses, proves to be an important step toward high-quality electron sources [34].

The photoemission process from a semiconductor photocathode can be best understood by Spicer's three-step model, which divides the behaviors of photoelectrons into the following three stages: generation, transport, and emission [35], [36]. The transport stage is the most complex one among the three, with critical implications to the time response and quantum yield of devices [37], [38]. It involves not only electrons migrating toward device surfaces but also their cooling and recombination along the process. Measurements made with both bulk and thin-film GaAs samples have shown that electrons excited into the conduction band thermalize very quickly to the bottom of the conduction band and the transport process can be very well described by the thermal diffusion model [31], [32], [35]. Several groups have studied photo-electron diffusion in GaAs photocathodes by characterizing time-resolved profiles of the emitted electron bunches [31]–[34]. Notably, Hartmann *et al*. reported the first high-precision measurement of temporal profiles of picosecond electron bunches from an NEA GaAs photocathode using a synchronized spatial pulse imaging system [31]. They also developed an electron diffusion model that has been widely adapted in subsequent research. The same group later reported

Manuscript received August 7, 2019; revised November 20, 2019 and December 11, 2019; accepted December 16, 2019. Date of publication December 19, 2019; date of current version January 9, 2020. This work was supported in part by the National Science Foundation (NSF) under Grant ECCS-1254902 and Grant ECCS-1606836, in part by the National Natural Science Foundation of China under Grant 61775203, and in part by the National Key Research and Development Program of China under Grant 2017YFF0210800. *(Corresponding author: Lingze Duan.)*

H. Jani and L. Duan are with the Department of Physics and Astronomy, The University of Alabama in Huntsville, Huntsville, AL 35899 USA (e-mail: lingze.duan@uah.edu).

L. Chen is with the Institute of Optical and Electronic Technology, China Jiliang University, Hangzhou 310018, China.

Color versions of one or more of the figures in this article are available online at http://ieeexplore.ieee.org.

Digital Object Identifier 10.1109/JQE.2019.2960774

characterization of response time and spin relaxation time of thin III-V photocathodes [32]. More recently, Honda *et al*. studied the effects of active layer thickness, boundary conditions and excitation wavelength on the temporal response of GaAs photocathodes [34], and Jin *et al*. investigated electron transportation in GaAs/GaAsP strained superlattice photocathodes [33]. Both works appear to validate the effectiveness of the diffusion model.

While these aforementioned efforts have resulted in considerable insight into the ultrafast carrier dynamics in GaAs photocathodes, their results are all based on *post-photoemission* measurement, which can only offer an *indirect* picture of photoelectron transport inside the devices. This is because emissions of photoelectrons strongly depend on surface conditions of the devices such as chemical compositions and scattering in the Cs/O activation layer [39], [40]. Since the activation layer is not involved in electron transport, a post-emission characterization may be heavily skewed by the emission conditions and hence fails to reflect the true properties of the diffusion process. This may explain the large discrepancies found in various reports about the measurement of diffusion coefficient [31], [34], [41], [42]. Moreover, post-emission characterization of photoelectron dynamics requires ultra-high vacuum environment and high bias voltages (>100 kV) [9], [34]. Such demanding conditions prevent the method from being widely applied.

In this paper, we demonstrate a simple yet effective approach to study photoelectron dynamics in GaAs photocathodes. The method is based on an optical technique called pump-probe reflectometry (PPR), which measures the ultrafast variations of reflectivity from a semiconductor sample upon the injection of a femtosecond excitation (or "pump") pulse [43]. Since the transient behavior of reflectivity is determined by the transient property of refractive index, which is closely related to carrier concentrations [44], [45], PPR is able to directly probe the accumulation of free carriers near the device surface. This provides a *pre-photoemission* scheme for the study of ultrafast photoelectron dynamics in GaAs photocathodes with femtosecond time resolutions [46]. Although PPR has long been used in solid-state physics to study material properties 47]–[52], it has not been directly applied on photocathodes, which typically feature layered doping structures to enhance carrier transport toward device surfaces. The potential of the method also rests upon its simplicity compared to the post-emission schemes. The measurement can be performed in the atmosphere with completely passive samples (no need to apply voltage). It is hoped that this proof-of-principle effort is able to outline a new pathway toward understanding the dynamics of III-V photocathodes, which can ultimately lead to better device architectures and performances.

The rest of the paper is organized as follows. In Section 2, the experiment is described, including the photocathode device under study, the PPR measurement system, and the main experimental results. In Section 3, a two-layer carrier diffusion-accumulation model is attempted. In Section 4, the theoretical and experimental results are compared, and key carrier transport and decay parameters are extracted. This is followed by discussions in Section 5 and, finally, conclusions in Section 6.

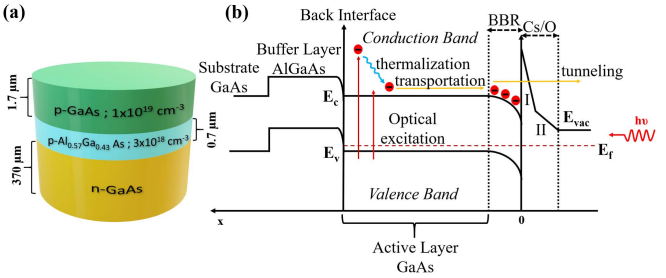

Fig. 1. (a) Doping structure of the tested GaAs/AlGaAs photocathode with a uniformly doped *p*-GaAs as the active layer. (b) The band scheme of typical GaAs NEA photocathodes, with the definitions of active layer and band bending region.

II. PPR Experiment

A. Photocathode Device

The photocathode used in this study is a GaAs/AlGaAs device fabricated with metal organic chemical vapor deposition (MOCVD) [53]. Its doping structure is shown in Fig. 1(a). A 0.7-μm layer of p-$Al_{0.57}Ga_{0.43}As$ with a doping concentration of 3×10^{18} cm^{-3} is directly grown on Si-doped GaAs (370 μm) substrate to serve as the buffer layer. Grown on top of the buffer layer is the active layer, which is 1.7 μm of p-GaAs *uniform-doped* at 1×10^{19} cm^{-3}. The surface of the device was activated with Cs/O.

Fig. 1(b) describes the band structure of a typical GaAs NEA photocathode and it clearly signifies each step involved in the photoemission process as described by Spicer's 3-step model [36]. The first step is the excitation of electrons from the valence band to the conduction band following the absorption of an optical pulse. The second step is the transport of excited electrons to the surface, during which the excited electrons scatter with phonons and other electrons, losing energy and thermalizing towards the conduction band minima. The active layer (p-doped GaAs bulk layer) is uniformly doped and hence there is no built-in electric field. As a result, the main mechanism by which the electrons move towards the surface is diffusion. Due to the presence of surface states, the energy bands of heavily p-doped GaAs bent downward near the surface [20]. This so-called band bending region effectively serves as a potential well for electrons, trapping the photoelectrons that have diffused into the vicinity of the surface. This diffusion-accumulation picture underlies our theoretical model, which will be discussed in detail later. The third and the final step is the emission of electrons. With the Cs/O surface-activation layer, the vacuum level falls below the bulk conduction band minima, allowing some of the photoelectrons trapped in the band bending region to escape into vacuum. Some electrons that are excited close to the surface can also reach vacuum without complete thermalization.

B. PPR System

A schematic of our PPR experimental system is shown in Fig. 2. Both the pump and the probe pulses are generated

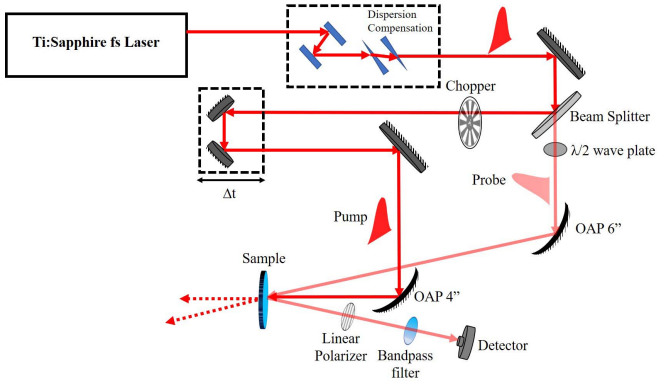

Fig. 2. Layout of the PPR setup. OAP: off-axis parabolic reflector.

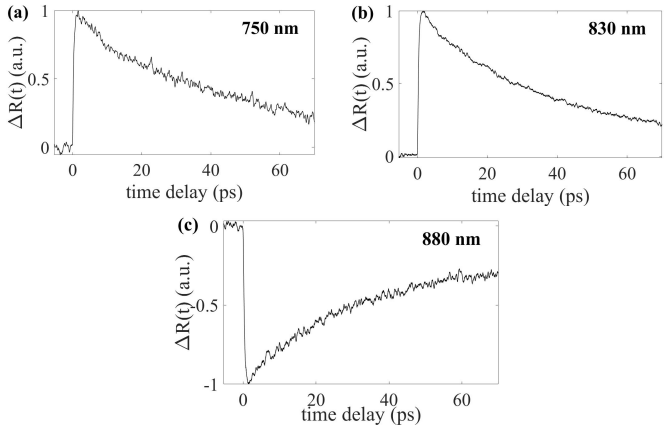

Fig. 3. The transient behaviors of reflectivity are revealed by PPR traces measured at three different wavelengths: (a) 750 nm, (b) 830 nm, and (c) 880 nm.

by a mode-locked Ti:sapphire laser (Venteon Pulse:One PE) with a repetition rate of 83 MHz, a pulse width of about 10 fs, and an average output power of 540 mW. A dispersion-adjustment unit at the output of the laser, which consists of dispersion-compensating mirrors and wedges, helps shape the pulses that arrive on the device surface. A broadband, dispersion-balanced beamsplitter splits the laser beam into the pump and the probe paths. The pump beam passes through a beam chopper and a motorized tunable delay line. The probe beam, which is more than 10 times weaker than the pump beam, has its polarization rotated by 90° (s-polarized) through a half-wave plate to avoid unwanted interference with the pump beam (p-polarized). Both beams are focused on the photocathode device surface with off-axis parabolic reflectors with the pump spot size about 3 times greater than the probe spot size. The two beams are slightly angled (15°) with respect to each other and the probe beam reflected off the device surface passes through a linear polarizer to remove the scattered pump beam before impinging on a Si photodetector. In addition, an optical bandpass filter is placed in front of the photodetector to select the center detection wavelength. The detector output feeds into a lock-in amplifier, which selectively amplifies the pump-pulse-induced modulation to the reflected probe power at various relative pulse delays. The relative change of the device reflectivity can be evaluated by normalizing the detected probe power variation to an independently calibrated nominal probe power.

C. Transient Behaviors of Reflectivity

PPR measurement has been taken on the photocathode at a number of probe wavelengths. Fig. 3 shows the measurement results at three representative wavelengths: one far above the GaAs band gap at 750 nm, one right above the band gap at 830 nm, and one below the band gap at 880 nm. In each case, a 10-nm bandpass filter is inserted in front of the photodetector to select the detection wavelength (see Fig. 2). The PPR traces in all three cases show a sharp leading edge after the injection of the pump pulse (at time zero), followed by a gradual decay. The initial change of reflectivity is positive at 750 nm and 830 nm but is negative at 880 nm. This sign difference across the band gap is a consequence of refractive index nonlinearity near the GaAs band gap [44], [45] and is consistent with prior observations made with bulk GaAs [48], [51].

A closer look at the traces in Fig. 3 shows that the reflectivity rises to 80% of its peak value in a period of about 500 fs. After that, the increase gradually slows down. At about 2 ps, the reflectivity reaches its peak value. It then begins a gradual decay, dropping to half of its peak value within 30 ps.

The above behaviors of reflectivity appear to be qualitatively consistent with a simple physical picture. The initial rise of the reflectivity is likely caused by the photo-generated free electrons near the surface. The electrons generated deeper inside the active layer diffuse toward the surface, causing the reflectivity to continue to rise. On the other hand, once the free-electron population reaches a certain level, bulk and surface recombination take over as the dominant processes, causing the free-electron population to decline and leading to a gradual reduction of reflectivity. However, this decline appears to be more complicated than a simple exponential decay, which indicates that there may be multiple mechanisms involved. One such mechanism has to do with the wavelength dependence of absorption coefficient α. Since the pump-pulse spectrum is quite broad, there is a diverse distribution of absorption length α^{-1} within the pump spectrum [54]. As a result of this $\alpha(\lambda)$ relation, longer wavelengths can penetrate deeper into the active layer and the generated photoelectrons need more time to diffuse into the surface region, potentially slowing down the decay of free-electron population on the surface. Another possible mechanism unique to NEA photocathodes is surface emission, which allows free electrons on the device surface to escape out of the device. It may provide an additional channel for the device to lose free electrons.

III. Theoretical Model

To quantitatively verify the above physical understanding, we have developed a carrier-diffusion model to explain the transient behaviors of reflectivity. Similar diffusion-based treatments have been widely adopted in the analysis of post-emission photoelectron dynamics [31]–[34]. The focus of the current study, however, is on pre-photoemission free-electron accumulation near the device surface.

Specifically, we divide the heavily p-doped GaAs layer into two distinctive sub-layers: a wide *active layer* (AL) where

most photoelectron generation and transport take place, and a very thin *band-bending region* (BBR) near the surface where photoelectrons accumulate after diffusion and become trapped. The two layers are conceptually illustrated in Fig. 1(b). In both layers, a general continuity equation can be written as

$$\frac{\partial n(\mathbf{r},t)}{\partial t} + \nabla \cdot \mathbf{J}(\mathbf{r},t) = G(\mathbf{r},t) - \Gamma n(\mathbf{r},t) \tag{1}$$

where $n(\mathbf{r},t)$ is electron concentration as a function of space and time, $\mathbf{J}(\mathbf{r},t)$ is electron flux, $G(\mathbf{r},t)$ describes electron generation by photo-excitation, and Γ is electron decay rate, which combines all the effects that lead to the reduction of photoelectron population.

Between the two layers, the BBR is treated as an infinitely thin layer of electron "sink". All the electrons diffusing into the BBR are trapped in it without any returning back to the AL. This assumption is justified because ***i***) the BBR has been shown to be about 10-70 nm wide for typical doping levels [37] (compared to 1-2 μm for the AL) so its impact on photoelectron generation is very small and ***ii***) the potential well formed within the BBR can effectively trap electrons, making electrons less likely to diffuse back into the AL. With this assumption, the analysis of photoelectron generation and diffusion is contained only within the AL, while the BBR contributes a Dirichlet boundary condition near the device surface [31]. The inner boundary of the AL interfaces with the AlGaAs buffer layer, which forms a potential barrier for photoelectrons, as shown in Fig. 1(b), and hence results in a Neumann boundary condition. We further argue that photoelectron generation by femtosecond pulses can be treated as an instantaneous process, which sets up an initial distribution of electron population. The ensuing photoelectron transport is a diffusion process based on this initial condition and the boundary conditions. In addition, it is mathematically convenient and valid to lump all the electron population decay into the BBR and treat the diffusion in the AL as decay-free. Neglecting any transverse inhomogeneity of the electron population, the only change to the electron flux occurs along the longitudinal direction x (i.e. depth from the device surface, as indicated in Fig. 1(b)). Thus, $\mathbf{J}(\mathbf{r},t)$ can be replaced by $\mathbf{J}(x,t) = -D[\partial n(x,t)/\partial x]\mathbf{x}$, where D is the diffusion coefficient. The continuity Eq. (1) is then reduced to a one-dimensional diffusion equation

$$\frac{\partial n(x,t)}{\partial t} = D\frac{\partial^2 n(x,t)}{\partial x^2} \tag{2}$$

with the initial condition $n(x, t=0) = n_0 e^{-\alpha x}$ and boundary conditions $n(x=0,t) = 0$ and $\partial n(x=d,t)/\partial x = 0$. Here d is the thickness of AL and α is the absorption coefficient of AL.

The general solution to this equation is,

$$n(x,t) = 2n_0 \sum_{i=1}^{\infty} b_i \sin(a_i x)\, e^{-a_i^2 Dt}, \quad t > 0 \tag{3}$$

where the expansion coefficients a_i and b_i can be derived from the initial conditions as

$$a_i = \frac{(2i-1)\pi}{2d} \quad and \quad b_i = \frac{a_i + (-1)^i \alpha e^{-\alpha d}}{d\left(\alpha^2 + a_i^2\right)} \tag{4}$$

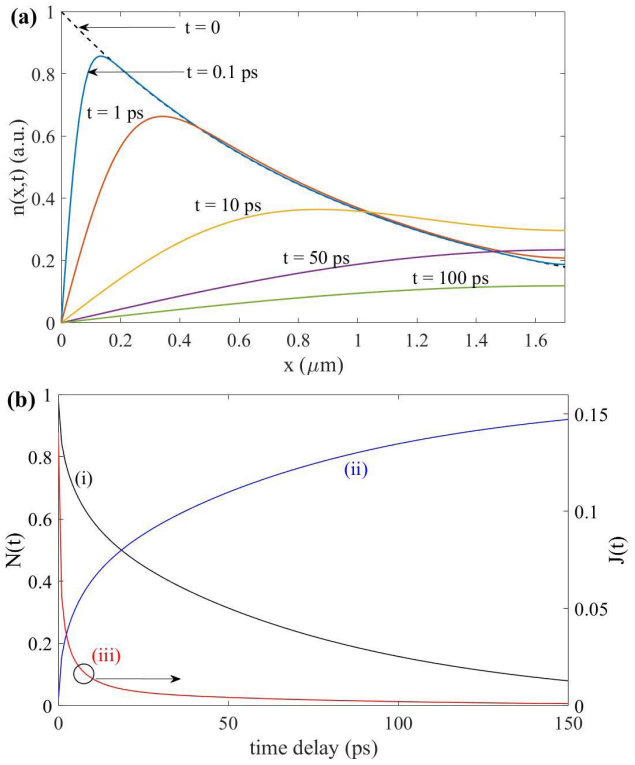

Fig. 4. Diffusion of photoelectrons inside the active layer: (a) time evolution of the electron concentration distribution in the AL; (b) total electron population and flux: (i) total electron population inside the AL as a function of time, (ii) total electron population injected from the AL into the BBR, and (iii) total electron flux injecting into the BBR as a function of time.

Fig. 4(a) shows the initial distribution of electron concentration $n(x, t=0)$ and several subsequent distribution curves at various time delays. An AL thickness of 1.7 μm has been used in these calculations to reflect the actual dimension of the tested device. All curves have been normalized to n_0. It should be noted here that, in order for the computation result to best simulate our experiment, the photoelectron distributions have been computed with the consideration of the broadband nature of femtosecond pulses. Specifically, the relative optical excitation power at different wavelengths have been derived from the actual pump pulse spectrum and the wavelength-dependent absorption coefficient $\alpha(\lambda)$ for GaAs has been taken into account [37]. The traces demonstrate the time-evolution of electron concentration in the AL as electrons gradually migrate from the AL into the BBR. The total electron population inside the AL, $N(t)$, which corresponds to the integral of $n(x,t)$ across the entire AL, exhibits a monotonic decrease over time as shown in Fig. 4 (b) (Trace (i)). The total number of electrons injected into the BBR, on the other hand, monotonically increases as illustrated by Trace (ii) in Fig. 4(b). The AL-to-BBR injection flux at any given time can be defined as $J(t) = -dN(t)/dt$ and is shown in Fig. 4(b) as Trace (iii). The photoelectron injection from the AL to the BBR is very strong immediately following the excitation but quickly tapers off after just a few picoseconds. This behavior is consistent with our experimental observation as will be discussed in the next section.

Moving on to the BBR, we once again begin with the continuity Eq. (1). Taking the integral $\int dx$ from $x = 0^-$ to $x = 0^+$ (i.e. across the thickness of the BBR) on both sides of Eq. (1) and neglecting the generation term $G(\mathbf{r}, t)$ as discussed earlier yield a modified continuity equation for the BBR:

$$\frac{\partial S(t)}{\partial t} = J(t) - \Gamma S(t), \tag{5}$$

where $S(t)$ is the total free-electron population in the BBR (averaged over the surface area).

The general solution of Eq. (5) is given by,

$$S(t) = \int_0^t J(\tau)\, e^{-\Gamma(t-\tau)} d\tau, \tag{6}$$

where $J(\tau) = -dN(\tau)/d\tau$. Combining Eq. (3) and Eq. (6), the general solution for $S(t)$ is found to be,

$$S(t) = 2n_0 D \sum_{i=1}^{\infty} b_i a_i \left(\frac{e^{-Da_i^2 t} - e^{-\Gamma t}}{\Gamma - Da_i^2} \right) \tag{7}$$

where the expansion coefficients a_i and b_i are defined in Eq. (4) In the case of multi-exponential decay, the overall population $S(t)$ can be divided into several sub-groups, with $S(t) = \sum S_j(t)$. Each $S_j(t)$ has its corresponding Γ_j (or, equivalently, carrier lifetime) and $J_j(t)$. Then Eq. (5), (6) and (7) can simply be used to solve for each $S_j(t)$ and all the sub-groups combine to give the overall population behavior.

The free electrons in the BBR alter the dielectric constant near the device surface, causing the surface reflectivity to change. The simplest model to describe this relation is the classical Drude theory [55], [56], which predicts the complex dielectric constant $\epsilon(\omega, t)$ as a function of free-carrier density as

$$\epsilon(\omega, t) = \epsilon_r(\omega) + \frac{e^2 S(t)}{m^* \epsilon_0 w} \frac{i\tau_e}{\omega(1 - i\omega\tau_e)}, \tag{8}$$

where e is the electron charge, ω is angular frequency, ϵ_0 is vacuum permittivity, m^* is effective mass of electron, τ_e is mean collision time of free electrons, $\epsilon_r(\omega)$ is the relative dielectric constant due to inter-band transition and w is the effective thickness of the BBR. An important conclusion drawn from Eq. (8) is that the transient reflectivity $\Delta R(t)$ following the excitation of a femtosecond pulse is *proportional* to the accumulated free-electron population in the BBR$S(t)$. This establishes the foundation of the our PPR technique, i.e. by measuring $\Delta R(t)$ using a pump-probe scheme, one can directly observe the evolution of photoelectron population near the device surface. The result in turn can be used to understand transient carrier dynamics such as carrier diffusion and population decay as suggested by Eq. (7). It should be pointed out that the Drude model does have certain limitations. For example, it has been shown that the model works very well far above the band gap but fails to account for some key carrier effects such as band filling and band gap renormalization near the band gap [50]. A comprehensive theory for free-carrier effects near the band gap is much more complicated and hence out of the scope of the current work [44], [50], [52]. However, the proportionality between $\Delta R(t)$ and $S(t)$ is believed to be a reasonable approximation regardless the Drude model is valid or not. Thus, the effectiveness of the PPR approach should not be affected by the particular model used here.

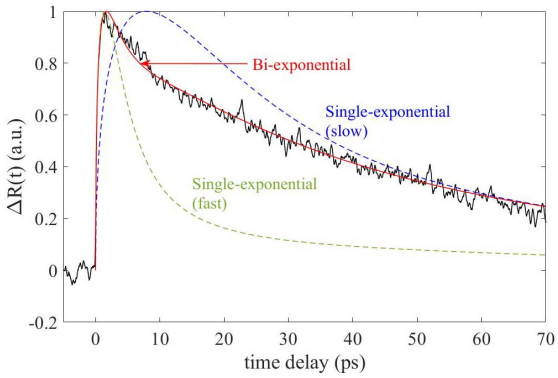

Fig. 5. Measured transient behaviors of reflectivity along with theoretical predictions based on single-exponential (dashed) and bi-exponential (solid) population-decay models.

IV. Theory-Experiment Comparisons

The direct correlation between $S(t)$ and $\Delta R(t)$ allows Eq. (7) to be directly compared with the experimentally measured transient reflectivity. This has been done by applying material and device parameters to Eq. (7) with proper assumptions to the electron decay rate Γ. One important finding through such comparisons is that a simple exponential decay of the free electron population is unable to explain the observed transient behaviors of the reflectivity. This is illustrated in Fig. 5, where two special cases of the theoretical curve are plotted against an experimental trace (measured at 750 nm). Both theoretical curves are obtained with a single decay rate Γ, the first one (fast) chosen to match the experimental trace at the peak reflectivity and the second one (slow) at the tail end. Evidently, neither curve can properly describe all the characteristics of the measured reflectivity. To address this problem, a biexponential decay model has been adopted, where the relaxation of the free-electron population in the BBR takes the form

$$S(t) \propto A \exp(-t/\tau_A) + B \exp(-t/\tau_B) \tag{9}$$

Here τ_A and τ_B are the carrier lifetimes of two independent decay processes; A and B are constants and satisfy the condition $A + B = 1$. With the additional degrees of freedom, a much better agreement between the numerical result and the experimental data has been achieved, as demonstrated by the solid red trace in Fig. 5.

The comparisons between experiment and theory also enable quantitative evaluation of key carrier dynamic parameters such as the electron diffusion coefficient D and the free-electron lifetimes τ_A and τ_B. Such assessment can potentially offer valuable physical insight into the dynamic properties of GaAs photocathodes. This has been done by optimizing the relevant parameters, namely D, τ_A,τ_B, A and B, so that the theoretical curves match the experimental traces. To minimize possible errors caused by ambiguous choices of parameters, the same set of theoretical values are used to fit all three

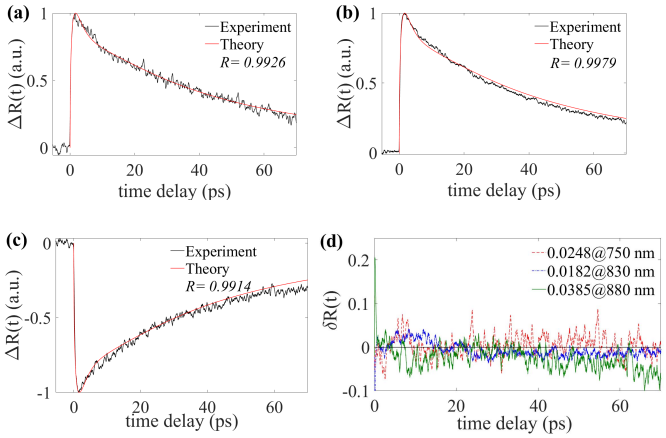

Fig. 6. Theoretical model is fit to experimental data measured at three different wavelengths, (a) 750 nm, (b) 830 nm, and (c) 880 nm, to determine the diffusion coefficient D and free-electron lifetimes τ_A and τ_B. Pearson correlation function R is calculated in each case to evaluate theory-experiment agreement. (d) The difference between the theoretical and experimental traces, denoted as δR(t), is plotted over the entire time span for all three wavelengths. The corresponding RMS errors are also included.

experimental traces shown in Fig. 3. The optimum matches are achieved with the following parameter values: $D = 160$ cm^2/s, $\tau_A = 1.56$ ps, $\tau_B = 21.60$ ps, $A = 0.76$ and $B = 0.24$, and the resulted experiment-theory comparisons are shown in Fig. 6. In all three cases, excellent agreement between theory and experiment is achieved as evident from the computed Pearson correlation function R. Furthermore, the difference between the experimental and the theoretical results across the full time span is plotted in Fig. 6(d). At all three wavelengths, this difference remains small over the entire span, as evident from the corresponding root-mean-square (RMS) errors.

V. Discussion

Several important conclusions can be drawn from the above results. The bi-exponential behavior of reflectivity indicates that there are at least two independent processes causing the reduction of free-electron population in the surface region, and their corresponding lifetimes are on the order of 1 ps and 20 ps, respectively. This characteristic of two decay times appears to agree with previous observation based on temporal measurement of emitted electron bunches [33]. Given the complexity of potential processes involved, the specific mechanisms underlying the two decay times are not completely clear based on the current experimental results. Prior reports have indicated that surface recombination in the BBR leads to a characteristic response time on the order of 1 ps [32] and the photoemission process from photocathodes with a similar active-layer thickness typically takes about tens of picoseconds [13], [32], [34]. Therefore, it is reasonable to conceive that surface recombination in the BBR and photoemission may have been the key processes underlying the bi-exponential behavior of reflectivity, although such an assessment will need further experimental verification. Meanwhile, the PPR-measured diffusion coefficient appears to agree with prior observation by Hartmann *et al.* [31], but larger than some other previously reported D values [32]–[34]. Given the pre-photoemission nature of PPR measurement, we believe this result indeed makes a strong case for considering greater free-electron diffusion in actual GaAs photocathodes. Finally, it should be noted that temperature change caused by pump power injection may also induce refractive index change on the device surface [57]. This effect, however, does not affect the observation of transient reflectivity since temperature-induced index change only depends on the average optical power of the pump beam, which remains constant in the experiment and can be easily removed during data processing. Similar argument can be made with regard to the incident angle of the probe beam, which is set at about 15° in our current setup. Although changing this angle may affect the reflected spectrum [58], it would not change the measured transient behaviors shown in Fig. 3 and Fig. 6 since it is a steady-state effect.

VI. Conclusion

In conclusion, we report the first pre-photoemission characterization of ultrafast photoelectron dynamics in GaAs photocathodes using pump-probe measurement of transient reflectivity. A diffusion model based on a two-layer assumption proves to be effective in explaining the experimental results. The free-electron population inside the band-bending region is found to experience bi-exponential decay. The diffusion coefficient in the active layer and the bi-exponential electron lifetimes are evaluated by comparing the theoretical model with the PPR measurement at multiple wavelengths. The result shows that $D = 160$ cm^2 /s, which is close to the diffusion coefficient of undoped GaAs (200 cm^2 /s), and the two lifetimes are on the orders of 1 ps and 20 ps, respectively. The PPR method and its results offer an alternative avenue toward understanding the temporal response of GaAs photocathodes and can potentially provide physical insight unattainable with conventional post-photoemission approaches.

Acknowledgment

The authors would like to thank the key support to this research by Dr. Y. Qian of the Nanjing Institute of Science and Technology, China, who supplied the photocathode device.

References

[1] R. A. L. Rue, K. A. Costello, C. A. Davis, J. P. Edgecumbe, and V. W. Aebi, "Photon counting III-V hybrid photomultipliers using transmission mode photocathodes," *IEEE Trans. Electron Devices*, vol. 44, no. 4, pp. 672–678, Apr. 1997.

[2] T. Maruyama *et al.*, "A very high charge, high polarization gradient-doped strained GaAs photocathode," *Nucl. Instrum. Methods Phys. Res. A, Accel. Spectrom. Detect. Assoc. Equip.*, vol. 492, nos. 1–2, pp. 199–211, Oct. 2002.

[3] V. V. Bakin *et al.*, "Semiconductor surfaces with negative electron affinity," *e-J. Surf. Sci. Nanotechnol.*, vol. 5, pp. 80–88, Mar. 2007.

[4] Z. Liu, Y. Sun, S. Peterson, and P. Pianetta, "Photoemission study of Cs-NF3activated GaAs(100) negative electron affinity photocathodes," *Appl. Phys. Lett.*, vol. 92, no. 24, Jun. 2008, Art. no. 241107.

[5] M. Suzuki *et al.*, "Real time magnetic imaging by spin-polarized low energy electron microscopy with highly spin-polarized and high brightness electron gun," *Appl. Phys. Express*, vol. 3, no. 2, Jan. 2010, Art. no. 026601.

[6] X. Chen, G. Tang, D. Wang, and P. Xu, "High quantum efficiency transmission-mode GaAlAs photocathode with a nanoscale surface structure," *Opt. Mater. Express*, vol. 8, no. 10, pp. 3155–3162, Oct. 2018.

[7] S. M. Gruner *et al.*, "Energy recovery linacs as synchrotron radiation sources (invited)," *Rev. Sci. Instrum.*, vol. 73, no. 3, p. 1402, 2002.

[8] I. V. Bazarov and C. K. Sinclair, "Multivariate optimization of a high brightness dc gun photoinjector," *Phys. Rev. Accel. Beams*, vol. 8, no. 3, pp. 88–101, 2005.

[9] I. V. Bazarov *et al.*, "Thermal emittance and response time measurements of negative electron affinity photocathodes," *J. Appl. Phys.*, vol. 103, no. 5, 2008, Art. no. 054901.

[10] T. Nishitani, M. Tabuchi, Y. Takeda, Y. Suzuki, K. Motoki, and T. Meguro, "High-brightness spin-polarized electron source using semiconductor photocathodes," *Jpn. J. Appl. Phys.*, vol. 48, no. 6, pp. 5–7, 2009.

[11] S. Karkare *et al.*, "Ultrabright and ultrafast III-V semiconductor photocathodes," *Phys. Rev. Lett.*, vol. 112, no. 9, pp. 1–5, 2014.

[12] P. Musumeci *et al.*, "Advances in bright electron sources," *Nucl. Instrum. Methods Phys. Res. A, Accel. Spectrom. Detect. Assoc. Equip.*, vol. 907, pp. 209–220, Nov. 2018.

[13] S. Hang, Y. Liu, H. Li, X. Tang, and D. Chen, "Temporal characteristic analysis of laser-modulated pulsed X-ray source for space X-ray communication," *Nucl. Instrum. Methods Phys. Res. A, Accel. Spectrom. Detect. Assoc. Equip.*, vol. 887, pp. 18–26, Apr. 2018.

[14] O. E. Tereshchenko *et al.*, "Solar energy converters based on multijunction photoemission solar cells," *Sci. Rep.*, vol. 7, no. 1, pp. 1–9, 2017.

[15] G. Wang *et al.*, "Thermally enhanced photoelectric emission from GaAs photocathode," *Sol. Energy*, vol. 174, pp. 352–358, Sep. 2018.

[16] K. Xu *et al.*, "Light emission from a poly-silicon device with carrier injection engineering," *Mater. Sci. Eng. B*, vol. 231, pp. 28–31, May 2018.

[17] K. Xu, "Silicon MOS optoelectronic micro-nano structure based on reverse-biased PN junction," *Phys. Status Solidi*, vol. 216, no. 7, Apr. 2019, Art. no. 1800868.

[18] J. Xue *et al.*, "Thermally enhanced blue light-emitting diode," *Appl. Phys. Lett.*, vol. 107, no. 12, Sep. 2015, Art. no. 121109.

[19] R. L. Bell and W. E. Spicer, "3-5 compound photocathodes: A new family of photoemitters with greatly improved performance," *Proc. IEEE*, vol. 58, no. 11, pp. 1788–1802, Nov. 1970.

[20] R. U. Martinelli and D. G. Fisher, "The application of semiconductors with negative electron affinity surfaces to electron emission devices," *Proc. IEEE*, vol. 62, no. 10, pp. 1339–1360, Oct. 1974.

[21] G. H. Olsen, D. J. Szostak, T. J. Zamerowski, and M. Ettenberg, "High-performance GaAs photocathodes," *J. Appl. Phys.*, vol. 48, no. 3, pp. 1007–1008, 1977.

[22] P. E. Gregory, J. S. Escher, R. R. Saxena, and S. B. Hyder, "Field-assisted photoemission to 2.1 microns from a Ag/p-$In_{0.77}$ $Ga_{0.23}$ As photocathode," *Appl. Phys. Lett.*, vol. 36, no. 8, pp. 639–640, Apr. 1980.

[23] J. Zou and B. Chang, "Gradient-doping negative electron affinity GaAs photocathodes," *Opt. Eng.*, vol. 45, no. 5, May 2006, Art. no. 054001.

[24] Z. Yang *et al.*, "Comparison between gradient-doping GaAs photocathode and uniform-doping GaAs photocathode," *Appl. Opt.*, vol. 46, no. 28, p. 7035, Oct. 2007.

[25] Y. Zhang *et al.*, "Influence of exponential-doping structure on photoemission capability of transmission-mode GaAs photocathodes," *J. Appl. Phys.*, vol. 108, no. 9, Nov. 2010, Art. no. 093108.

[26] Y. Zhang, J. Zou, J. Niu, J. Zhao, and B. Chang, "Photoemission characteristics of different-structure reflection-mode GaAs photocathodes," *J. Appl. Phys.*, vol. 110, no. 6, Sep. 2011, Art. no. 063113.

[27] Y. J. Zhang, J. Zhao, J. J. Zou, J. Niu, X. L. Chen, and B. K. Chang, "The high quantum efficiency of exponential-doping AlGaAs/GaAs photocathodes grown by metalorganic chemical vapor deposition," *Chin. Phys. Lett.*, vol. 30, no. 4, Apr. 2013, Art. no. 044205.

[28] A. V. Aleksandrov *et al.*, "Experimental study of the response time of GaAs as a photoemitter," *Phys. Rev. E, Stat. Phys. Plasmas Fluids Relat. Interdiscip. Top.*, vol. 51, no. 2, pp. 1449–1452, Feb. 1995.

[29] I. V. Bazarov *et al.*, "Efficient temporal shaping of electron distributions for high-brightness photoemission electron guns," *Phys. Rev. Accel. Beams*, vol. 11, no. 4, 2008, Art. no. 040702.

[30] J. S. Escher and H. Schade, "Calculated energy distributions of electrons emitted from negative electron affinity GaAs: CsSingle bond signO surfaces," *J. Appl. Phys.*, vol. 44, no. 12, pp. 5309–5313, Dec. 1973.

[31] P. Hartmann *et al.*, "A diffusion model for picosecond electron bunches from negative electron affinity GaAs photocathodes," *J. Appl. Phys.*, vol. 86, no. 4, pp. 2245–2249, 1999.

[32] K. Aulenbacher *et al.*, "Pulse response of thin III/V semiconductor photocathodes," *J. Appl. Phys.*, vol. 92, no. 12, pp. 7536–7543, 2002.

[33] X. Jin *et al.*, "Picosecond electron bunches from GaAs/GaAsP strained superlattice photocathode," *Ultramicroscopy*, vol. 130, pp. 44–48, Jul. 2013.

[34] Y. Honda *et al.*, "Temporal response measurements of GaAs-based photocathodes," *Jpn. J. Appl. Phys.*, vol. 52, no. 8R, Aug. 2013, Art. no. 086401.

[35] W. E. Spicer, "Negative affinity 3-5 photocathodes: Their physics and technology," *Appl. Phys.*, vol. 12, no. 2, pp. 115–130, Feb. 1977.

[36] W. E. Spicer and A. Herrera-Gomez, "Modern theory and applications of photocathodes," *Proc. SPIE*, vol. 2022, p. 18, Oct. 1993.

[37] S. Karkare *et al.*, "Monte Carlo charge transport and photoemission from negative electron affinity GaAs photocathodes," *J. Appl. Phys.*, vol. 113, no. 10, Mar. 2013, Art. no. 109901.

[38] Z. Cai, W. Yang, W. Tang, and X. Hou, "Numerical analysis of temporal response of a large exponential-doping transmission-mode GaAs photocathode," *Mater. Sci. Semicond. Process.*, vol. 16, no. 2, pp. 238–244, Apr-2013.

[39] D. C. Rodway and M. B. Allenson, "In situ surface study of the activating layer on GaAs (Cs, O) photocathodes," *J. Phys. D. Appl. Phys.*, vol. 19, no. 7, pp. 1353–1371, Jul. 1986.

[40] X. Chen *et al.*, "Photoemission characteristics of (Cs, O) activation exponential-doping $Ga_{0.37}Al_{0.63}As$ photocathodes," *J. Appl. Phys.*, vol. 113, no. 21, p. 213105, Jun. 2013.

[41] J. S. Blakemore, "Semiconducting and other major properties of gallium arsenide," *J. Appl. Phys.*, vol. 53, no. 10, pp. R123–R181, Oct. 1982.

[42] K. Beyzavi, K. Lee, D. M. Kim, M. I. Nathan, K. Wrenner, and S. L. Wright, "Temperature dependence of minority-carrier mobility and recombination time in p-type GaAs," *Appl. Phys. Lett.*, vol. 58, no. 12, pp. 1268–1270, 1991.

[43] C. A. D. Roeser *et al.*, "Femtosecond time-resolved dielectric function measurements by dual-angle reflectometry," *Rev. Sci. Instrum.*, vol. 74, no. 7, pp. 3413–3422, Jul. 2003.

[44] Y. H. Lee *et al.*, "Room-temperature optical nonlinearities in GaAs," *Phys. Rev. Lett.*, vol. 57, no. 19, pp. 2446–2449, Nov. 1986.

[45] B. R. Bennett, R. A. Soref, and J. A. Del Alamo, "Carrier-induced change in refractive index of InP, GaAs and InGaAsP," *IEEE J. Quantum Electron.*, vol. 26, no. 1, pp. 113–122, Jan. 1990.

[46] L. Chen, L. Duan, and H. P. Jani, "Femtosecond pump-probe study of negative electron affinity GaAs/AlGaAs photocathodes," in *Proc. SPIE*, vol. 10530, Feb. 2018, Art. no. 105300X.

[47] C. V. Shank, R. Yen, and C. Hirlimann, "Time-resolved reflectivity measurements of femtosecond-optical-pulse-induced phase transitions in silicon," *Phys. Rev. Lett.*, vol. 50, no. 6, pp. 454–457, Feb. 1983.

[48] R. Yano, Y. Hirayama, S. Miyashita, H. Sasabu, N. Uesugi, and S. Uehara, "Pump-probe spectroscopy of low-temperature grown gaAs for carrier lifetime estimation: Arsenic pressure dependence of carrier lifetime during MBE crystal growth," *Phys. Lett. A*, vol. 289, nos. 1–2, pp. 93–98, Oct. 2001.

[49] A. J. Sabbah and D. M. Riffe, "Femtosecond pump-probe reflectivity study of silicon carrier dynamics," *Phys. Rev. B, Condens. Matter Mater. Phys.*, vol. 66, no. 16, pp. 1–11, Oct. 2002.

[50] S. S. Prabhu and A. S. Vengurlekar, "Dynamics of the pump-probe reflectivity spectra in GaAs and GaN," *J. Appl. Phys.*, vol. 95, no. 12, pp. 7803–7812, Jun. 2004.

[51] S. Janz, U. G. Akano, and I. V. Mitchell, "Nonlinear optical response of As+-ion implanted GaAs studied using time resolved reflectivity," *Appl. Phys. Lett.*, vol. 68, no. 23, p. 3287, Jun. 1995.

[52] N. P. Wells, P. M. Belden, J. R. Demers, and W. T. Lotshaw, "Transient reflectivity as a probe of ultrafast carrier dynamics in semiconductors: A revised model for low-temperature grown GaAs," *J. Appl. Phys.*, vol. 116, no. 7, Aug. 2014, Art. no. 073506.

[53] X. Chen *et al.*, "Research on quantum efficiency of reflection-mode GaAs photocathode with thin emission layer," *Opt. Commun.*, vol. 287, pp. 35–39, Jan. 2013.

[54] Y.-F. Lao and A. G. Unil Perera, "Dielectric function model for p-type semiconductor inter-valence band transitions," *J. Appl. Phys.*, vol. 109, no. 10, May 2011, Art. no. 103528.

[55] T. Tanaka, A. Harata, and T. Sawada, "Subpicosecond surface-restricted carrier and thermal dynamics by transient reflectivity measurements," *J. Appl. Phys.*, vol. 82, no. 8, pp. 4033–4038, Oct. 1997.

[56] E. N. Glezer, Y. Siegal, L. Huang, and E. Mazur, "Laser-induced band-gap collapse in GaAs," *Phys. Rev. B, Condens. Matter*, vol. 51, no. 11, pp. 6959–6970, Mar. 1995.

[57] J. P. Kim and A. M. Sarangan, "Temperature-dependent Sellmeier equation for the refractive index of $Al_xGa_{1-x}As$," *Opt. Lett.*, vol. 32, no. 5, p. 536, Mar. 2007.

[58] K. Xu, Y. Chen, T. A. Okhai, and L. W. Snyman, "Micro optical sensors based on avalanching silicon light-emitting devices monolithically integrated on chips," *Opt. Mater. Express*, vol. 9, no. 10, pp. 3985–3997, Oct. 2019.

Hemang Jani (S'15) was born in Vadodara, India. He received the B.Sc. and M.Sc. degrees in physics from The Maharaja Sayajirao University of Baroda in 2008 and 2010, respectively, and the M.S. degree in physics from The University of Alabama in Huntsville (UAH) in 2013. In 2013, he joined the Precision Ultrafast Light Sciences (PULS) Group, UAH, where he is currently pursuing the Ph.D. degree in optical science and engineering. As a part of his research, he is using few-cycle Ti: sapphire laser to conduct pump-probe transient reflectivity experiments to study ultrafast carrier dynamics in novel semiconductors. He is currently an active Student Member of the IEEE Photonics Society, OSA, and SPIE. He has held several leadership positions in their student chapters.

Liang Chen received the master's and Ph.D. degrees in optical engineering from the Nanjing University of Science and Technology, Nanjing, China, in 2004 and 2011, respectively. He is currently an Associate Professor with the Institute of Optical and Electronic Technology, China Jiliang University, Hangzhou, China. His research interests include a wide area of optical technologies, including photoelectric materials and devices, low-light detectors and systems, and solar-blind UV photocathodes. He has published widely on GaAs theoretical research and surface activation techniques. He was a recipient of the China Scholarship Council (CSC) Fellowship in 2016, which supported his visit to The University of Alabama in Huntsville, Huntsville, AL, USA, from 2016 to 2017.

Lingze Duan (M'01–SM'14) was born in Beijing, China. He received the B.S. degree in physics from Tsinghua University, Beijing, China, in 1995, and the Ph.D. degree in electrical engineering from the University of Maryland, College Park, MD, USA, in 2002. From 2002 to 2004, he was a Post-Doctoral Associate with the Research Laboratory of Electronics (RLE), Massachusetts Institute of Technology, Cambridge, MA, USA, where he conducted research on octave-spanning optical pulse generation and characterization. From 2004 to 2007, he was a Post-Doctoral Researcher with the Department of Physics, Pennsylvania State University, University Park, where he developed ultrastable diode laser systems based on high-Q optical cavities. He joined the Department of Physics and Astronomy, The University of Alabama in Huntsville, Huntsville, AL, USA, as a Faculty Member, in 2007, where he has been an Associate Professor since 2013. He has authored or coauthored over 70 refereed technical publications. His research interests include ultrafast nanophotonics, frequency metrology with femtosecond frequency combs, fiber optic sensors, and novel applications of optics in astrophysics. He is a Senior Member of the Optical Society (OSA). He was a recipient of the National Science Foundation Faculty Early Career Development (CAREER) Award in 2013.